On the Dynamics of Dimpled Electrostatic MEMS Actuators

A.M. Alneamy*, M.S. Al-Ghamdi*, M. Khater**, B. Li*, R.S. Almikhlafi*, S. Park*,
E.M. Abdel-Rahman* and G.R. Heppler*
*Dept. of Systems Design Engineering, University of Waterloo, Waterloo, Canada
**Mechanical Engineering Dept., KFUPM, Dahran, Saudi Arabia

Summary. In this paper, we experimentally and analytically investigate the response of an electrostatic microplate actuator equipped with two anti-stiction dimples. We found that the introduction of dimples eliminates multi-valuedness from the actuator response and enables a tapping mode, in which the dimples make repeated contact with the landing pads. A lumped-mass model is developed to investigate the dynamic behavior of the actuator in flight and tapping modes. The model results were validated by comparison to experimental results. The model predicts period-doubling bifurcations and an intermittency route to chaos in the tapping mode regime.

Introduction

Electrostatic actuation is widely used in microelectromechanical systems (MEMS). It adds another layer of nonlinearity to their behavior, in addition to the inherent structural and damping nonlinearities. Stability and reliability issues, such as pull-in, stiction, and dielectric charging, are the main challenges to electrostatic actuators [1, 2]. Pull-in is a primary source of instability in electrostatic actuators, leading to stiction or dielectric charging of insulation layers. To over come these challenges, dimples are introduced to prevent stiction and dielectric charging. Yang *et al.* [3] demonstrated the use of dimples to reduce the actuation voltage of electrostatic shunt switches. Zhao *et al.* [4] showed that the effective nonlinearity of electrostatic actuators changes from softening to hardening once they come into impact with a hard-stop. In this paper, experiments were carried out to investigate the behaviour of an electrostatic actuator equipped with dimples. A model was also developed and validated to further investigate the actuator response.

Actuator Design

The actuator is made of gold in the UW-MEMS fabrication process [5]. It features two identical cantilever beams, ($l_b = 125\,\mu$m, $b_b = 10\,\mu$m), supporting a microplate, ($l_p = 120\,\mu$m, $b_p = 30\,\mu$m), and a common electrode placed underneath it, Fig. 1(a). Two dimples, ($10 \times 10\ \mu\text{m}^2$), fabricated on both sides of the microplate act as stoppers once they come into contact with matching landing pads fabricated into the substrate, Fig. 1(b). The nominal capacitive gap between the microplate and the bottom electrode, is d=3.7μm.

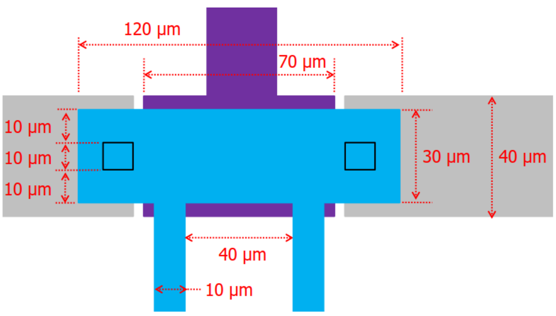

(a) Top view

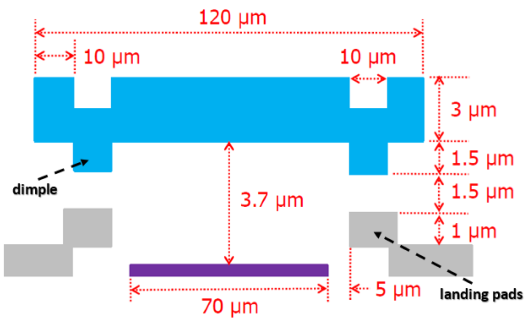

(b) Front view

Fig. 1: The actuator layout.

Lumped model

The plate is excited electrostatically by applying a voltage difference V between it and a fixed bottom electrode, Fig. 1. The actuator is modeled as a single-degree-of-freedom lumped model. The equation of motion describing the out-of-plane displacement of the microplate center $w(t)$ can be written as

$$m_{eq}\ddot{w} + (c_v + c_s)\dot{w} + k_{eq}w = \frac{\varepsilon A(V_{dc} + V_{ac}\cos(\Omega t)^2}{2(d-w)^2} \tag{1}$$

where m_{eq} is the effective mass, c_v is the viscous damping coefficient, c_s is the squeeze film damping coefficient, k_{eq} is the linear stiffness, ε is air permittivity, A is the common electrode area, V_{dc} is bias voltage, and V_{ac} and Ω are the amplitude and frequency of the ac voltage. The distance between the dimple and the landing pad is denoted w_{st} and subject to the impact condition is expressed as:

$$w(\dot{t}_{i^-}) = -ew(\dot{t}_{i^+}) \quad ; \quad w(t_i) = w_{st} \tag{2}$$

where e is a restitution coefficient.
The quality factor was measured experimentally $Q = 6.27 = \sqrt{k_{eq}m_{eq}}/c_v$ for the flight mode. We adopt Krylov's [6] model to represent the squeeze film damping under the microplate. The model assumes a uniform gap between two rigid plates, squeeze-film damping was found proportional to the cube of the distance between the movable plate and the substrate surface.

$$c_s = \frac{\hat{\mu}\, b_p^3}{(1+6K_n)(d-w)^3} \tag{3}$$

where $K_n = \lambda/d$ is Knudsen number, $\lambda = 60\,\text{nm}$ is the mean free path of air molecules at ambient pressure, and $\hat{\mu}$ is air viscosity. For convenience, we introduce nondimensional variables (denoted by over hats) to nondimensionlize the equation of motion:

$$\hat{w} = \frac{w}{d} \quad , \quad \hat{t} = \frac{t}{T} \tag{4}$$

where $T = \sqrt{m_{eq}/k_{eq}}$ is a time-scale. Substituting Eq. (4) into Eq. (1) and dropping the over hats for sake of succinctness, we obtain the non-dimensional equation of motion as:

$$\ddot{w} + (\mu_1 + \mu_2)\dot{w} + w = \frac{\alpha(V_{dc} + V_{ac}\cos(\Omega t)^2}{(1-w)^2} \tag{5}$$

where

$$\mu_1 = c_v\frac{T}{m_{eq}} \quad , \quad \mu_2 = \frac{\beta\mu}{(1-w)^3} \quad , \quad \mu = 0.42\frac{l_p\hat{\mu}}{m_{eq}}\left(\frac{b_p}{d}\right)^3\sqrt{\frac{k_{eq}}{m_{eq}}} \quad , \quad \beta = \frac{1}{1+6K_n} \quad , \quad \alpha = \frac{1}{2}\frac{\varepsilon A_p}{k_{eq}\,d^3}$$

Results and Discussion

Using an impulse signal with a frequency $f = 1\,\text{kHz}$ and a FFT spectrum of $[0; 100]\,\text{kHz}$, the first bending mode was measured experimentally as $\omega_n = 20.12\,\text{kHz}$. Two experiments were conducted on the actuator. In the first experiment, a frequency sweep carried out in the range of $[12-21]\,\text{kHz}$ with voltage amplitude set to $V_{ac} = 0.5\,\text{V}$ while the bias voltage V_{dc} was varied from 20 V to 28 V in steps of 2 V. Figure 2 shows the frequency-response curves of the microplate center velocity for this experiment. The shift in the natural frequency is due to the softening effect of the dc voltage on the actuator. The results show that no impact during this experiment.

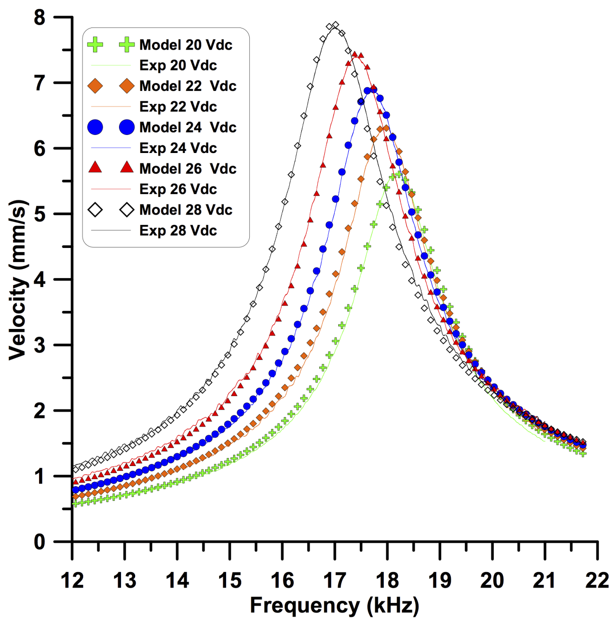

Fig. 2: The frequency-response curves of the actuator for $V_{ac} = 0.5\,\text{V}$

A good match was achieved between model predictions (solid lines) and experimental results (symbols) across all four actuation levels. As the actuator motions increased, the effective gap between the plate and substrate decreased which required a different squeeze-film damping parameter β for each excitation level. The parameters identified by matching model prediction to experimental measurements are listed in Table 1.
In the second experiment, a frequency sweep was carried out in the range of $[12-21]\,\text{kHz}$ with bias voltage set to $V_{dc} = 30\,\text{V}$ while the voltage amplitude V_{ac} was varied from 1.5 V to 5.5 V in steps of 1 V. As V_{ac} increased, the size of the actuator's flight mode motions increased until $V_{ac} = 5.5\,\text{V}$ where the dimples touched the landing pads and

Table 1: Squeeze-film damping parameter β

V_{dc}	V_{ac}	β	V_{dc}	V_{ac}	β
20	0.5	0.21	30	1.5	0.29
22	0.5	0.23	30	2.5	0.31
24	0.5	0.28	30	3.5	0.38
26	0.5	0.31	30	4.5	0.41
28	0.5	0.34	30	5.5	0.43
1^{st} experiment			2^{nd} experiment		

the actuator switched to tapping mode as shown in Fig. 3. Tapping occurred only in a small frequency range in the vicinity of the nonlinear resonance frequency. A good match was achieved between model predictions (solid lines) and

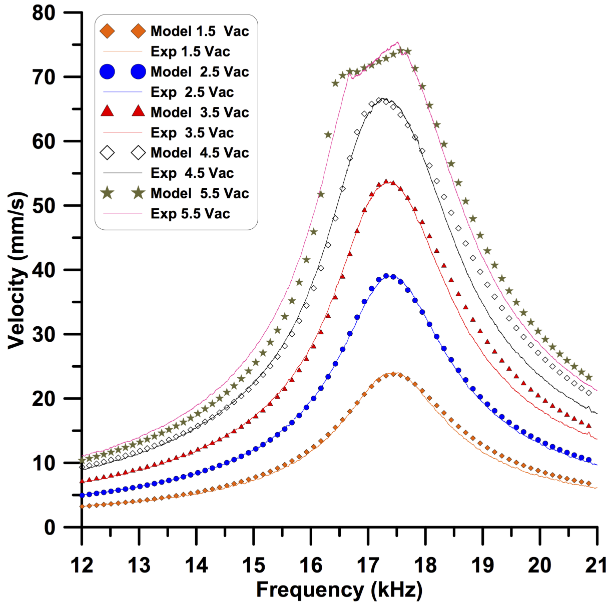

Fig. 3: The frequency-response curves of actuator for $V_{dc} = 30\,\text{V}$

experimental results (symbols) across all five actuation levels, thereby validating the model in both flight and tapping modes. During tapping mode, the model parameters were set as follows: restitution coefficient $e = 0.19$, separation distance $w_{st} = 1.39\,\mu$m, and quality factor $Q = 30$. The squeeze-film damping parameter β values used in the model are listed in Table 1. The model was then used to predict the actuator response when excited by a bias voltage $V_{dc} = 30\,\text{V}$ and

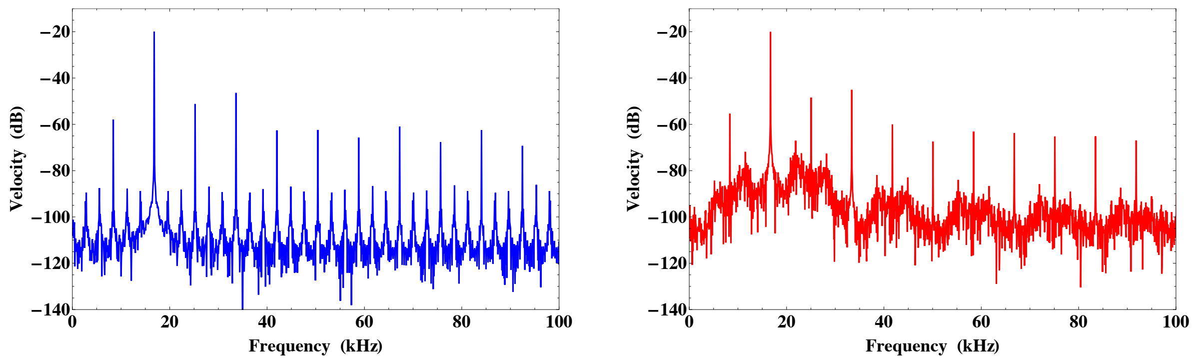

(a) FFT at $\Omega = 16.811\,\text{kHz}$ (b) FFT at $\Omega = 16.69\,\text{kHz}$

Fig. 4: The actuator response for the excitation signal $V_{dc} = 30\,\text{V}$ and $V_{ac} = 5.5\,\text{V}$

a signal amplitude and frequency of $V_{ac} = 5.5\,\text{V}$ and $\Omega = 16.811\,\text{kHz}$. First, the steady-state response of the actuator was obtained by numerically integrating the equation of motion, Eq. (5), for 600 excitation periods (T_s). Then, the FFT of the microplate center velocity $\dot{w}$ in the last 360 signal periods was evaluated, Fig. 4, where the dB scale set such that 0dB=1 m/s. The figure shows peaks at the excitation frequency Ω, half the excitation frequency $\frac{1}{2}\Omega$, and their integer multiples which is evidence of a period doubling bifurcation. Decreasing the excitation frequency to $\Omega = 16.69\,\text{kHz}$, the FFT shows a significant increase in the noise floor suggesting onset of chaos. This is expected in the presence of stretching, due to resonant electrostatic excitation, and folding due to dimple impacts.

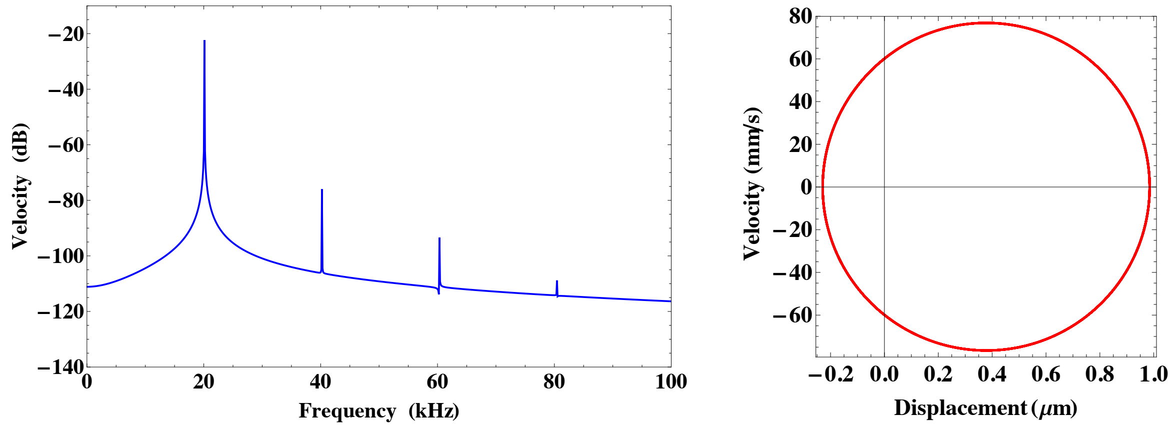

(a) FFT (b) Phase portrait

Fig. 5: The actuator response for the excitation signal $V_{dc} = 30\,\mathrm{V}$ and $V_{ac} = 7\,\mathrm{V}$, and $\Omega = 20\,\mathrm{kHz}$

We examined the actuator response at a higher excitation level with signal parameters: $V_{dc} = 30\,\mathrm{V}$ and $V_{ac} = 7\,\mathrm{V}$, and $\Omega = 20\,\mathrm{kHz}$. The FFT of the numerically predicted velocity $\dot{w}$, Fig. 5(a), was obtained using the procedure described above. It shows that the actuator response is in period-one (P-1) periodic flight mode. The corresponding single loop phase portrait of the orbit, Fig. 5(b), confirms this conclusion.

Decreasing the signal frequency to $\Omega = 15.68\,\mathrm{kHz}$ resulted in tapping mode response where the dimples came into contact with the landing pads. The FFT and the phase portrait of the steady-state orbit in this case, Fig. 6, indicate a period-doubling bifurcation resulting in a P-2 orbit with peaks appearing in the FFT at half of the excitation frequency and its integer multiples and a second loop appearing the the phase portrait. The phase portrait Fig. 6(b), shows that the actuator impacts the landing pads ($w_{st} = 1.39\,\mu\mathrm{m}$) every other signal cycle.

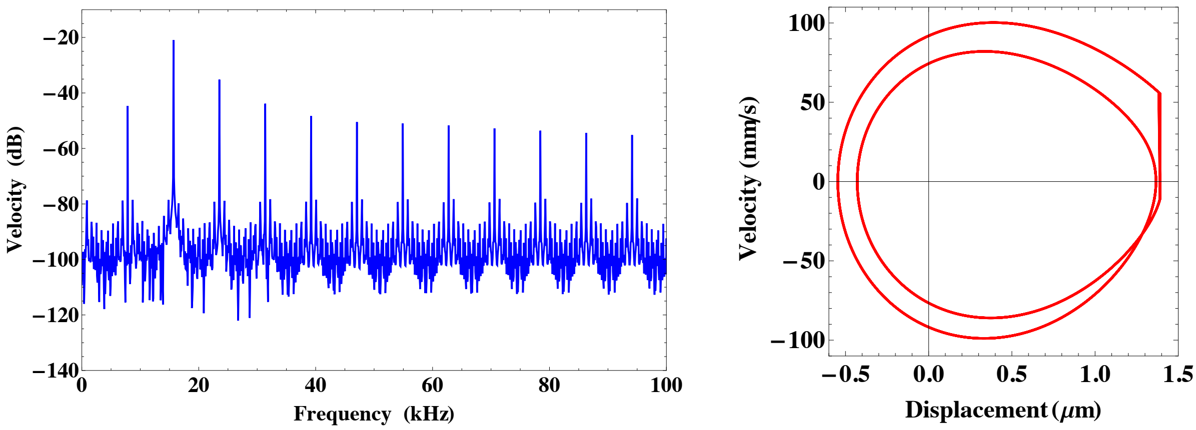

(a) FFT (b) Phase portrait

Fig. 6: The actuator response for the excitation signal $V_{dc} = 30\,\mathrm{V}$ and $V_{ac} = 7\,\mathrm{V}$, and $\Omega = 15.68\,\mathrm{kHz}$

Decreasing the excitation frequency further to $\Omega = 14.457\,\mathrm{kHz}$, aperiodic responses appeared characterized by bursts at irregular intervals typical for intermittent behavior, Fig. 7. The figure presents the time-histories of the numerically predicted displacement w and velocity $\dot{w}$ of the microplate center obtained numerically by integrating the equation of motion, Eq. (5), for $600T_s$ and recoding the last 360 signal periods. We found that the regularity of the bursts increase as the signal frequency increases. This is also typical of intermittent behavior, as it approaches fully developed chaos with bursts interrupting laminar flow more frequently at shorter intervals.

The corresponding FFT and phase portrait are shown in Fig. 8. The phase portrait reveals that the bursts represent impact events between the dimples and the landing pads which result in re-injection of the response and restarts laminar flow. Comparing Fig. 5(a) to Fig. 8(a), we note that the intermittent irregularity elevates the noise floor of the response from $-100\,\mathrm{dB}$ to $-80\,\mathrm{dB}$ which is an indicator of impending chaos.

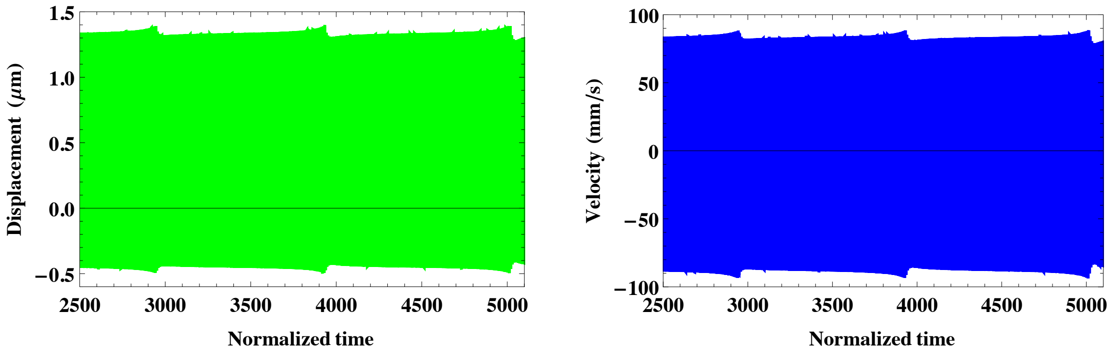

(a) Displacement (b) Velocity

Fig. 7: The actuator time-histories for the excitation signal $V_{dc} = 30\,\mathrm{V}$ and $V_{ac} = 7\,\mathrm{V}$, and $\Omega = 14.457\,\mathrm{kHz}$

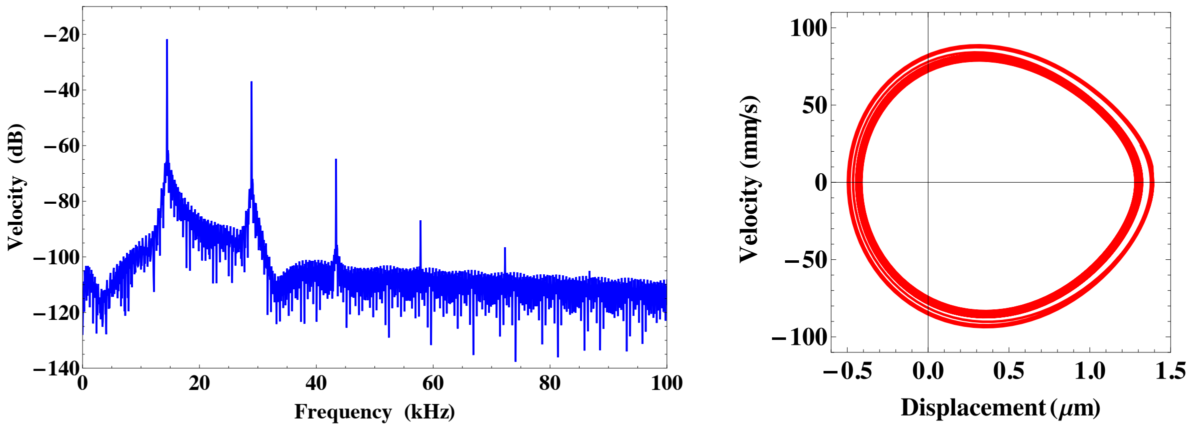

(a) FFT (b) Phase portrait

Fig. 8: The actuator response for the excitation signal $V_{dc} = 30\,\mathrm{V}$ and $V_{ac} = 7\,\mathrm{V}$, and $\Omega = 14.457\,\mathrm{kHz}$

Conclusions

The performance of an electrostatic MEMS actuator equipped with dimples was investigated in this paper. The actuator was fabricated using the UW-MEMS process. Results show that using dimples in electrostatic actuators can prevent pull-in, eliminate multivaluedness, and cyclic-fold bifurcations. On the other hand, it results in a new tapping operational mode. We developed and validated a model for the actuator encompassing tapping mode. Using this model, we found that period-doubling bifurcations and an intermittency route to chaos in the tapping mode regime.

References

[1] Sousa P. M., Chu V., Conde J. P. (2012) Reliability and stability of thin-film amorphous silicon MEMS resonators. Journal of Micromechanics and Microengineering **22**:065030.

[2] Zhu L., Xu J., Zhang Z., Hess D.W., Wong C.P. (2005) Lotus effect surface for prevention of microelectromechanical system (MEMS) stiction. In Proceedings of the IEEE Electronic Components and Technology, 2005. ECTC'05. pp. 1798-1801.

[3] Yang H.-H., Choi D.-H., Lee J.O., Yoon J.B. (2011) Modeling, fabrication and demonstration of an electrostatic actuator with a coplanar pre-charged electrode. Journal of Micromechanics and Microengineering **21**:085012.

[4] Zhang W., Turner K. L. (2005) Application of parametric resonance amplification in a single-crystal silicon micro-oscillator based mass sensor. Sensors and Actuators A: Physical **122**:23-30.

[5] UW-MEMS Design Handbook Version 2.0 Preliminary (2008). University of Waterloo. [Online]. Available: https://uwaterloo.ca/centre-integrated-rf-engineering/mems-process-design-handbook, accessed Apr. 28, 2017.

[6] Krylov, S. (2007). Lyapunov exponents as a criterion for the dynamic pull-in instability of electrostatically actuated microstructures. International Journal of Non-Linear Mechanics, 42(4), 626-642.